On the radiated noise computed by large-eddy simulation

C. Seror and P. Sagaut[a)]
ONERA 29 av. de la Division Leclerc, 92322 Châtillion Cedex, France

C. Bailly and D. Juvé
ECL-LMFA 36 av. Guy de Collongue, BP 163, 69131 Ecully Cedex, France

(Received 13 January 2000; accepted 6 November 2000)

This paper addresses the problem of the estimation of the noise radiated by forced isotropic turbulence using an hybrid large-eddy simulation/Lighthill analogy approach. The scale separation associated with the LES approach leads to splitting the acoustic source term as the sum of several contributions. The subgrid scale and high frequency contributions to radiated acoustic spectrum are first evaluated on the ground of filtered direct numerical simulations. The parametrization of subgrid scale effects based on a scale similarity model is addressed. Both *a priori* and *a posteriori* tests demonstrate the efficiency of the proposed model. © *2001 American Institute of Physics.*
[DOI: 10.1063/1.1336150]

I. INTRODUCTION

Sound generated by turbulence is an important source of noise and raises many questions of fundamental and engineering interest. A steady statistical description of the turbulent flow has long been used[1,2] before numerical simulations were carried out to compute the aerodynamic field.[3] Recent progress in computational fluid dynamics (CFD) now offers many tools to develop new techniques in computational aero-acoustics (CAA), but sound calculation and propagation is still a difficult numerical problem[4,5] because of the wide range of spatial and temporal frequencies.

Direct numerical simulation (DNS),[6] unsteady Reynolds-averaged Navier–Stokes simulations (RANS),[7] semi-deterministic modeling (SDM)[8,9] or, as detailed in this paper, large-eddy simulation (LES),[10,11] are currently used to compute the acoustic source (i.e., the unsteady flow field). All the methods described below offer many possibilities but also have some drawbacks: DNS yields a complete representation of the acoustic source term but does not offer the possibility to compute the high Reynolds number turbulent flow that must be dealt with in practice. On the contrary RANS allows access to very high Reynolds number turbulent flows but can only compute the coherent structures. LES, which is an intermediary method consisting of computing only the largest scales, has received a growing interest over the last years. The turbulent motion and the acoustic field can be computed in the entire computational domain but this method becomes rapidly very expensive and cannot be used for engineering problems. A hybrid method, based on computation of the aerodynamic fluctuations by solving Navier–Stokes equations, and on the calculation of the radiated noise by acoustic analogy is often preferred. Acoustic analogies are numerous and only a few of them are recalled here: Lighthill's analogy[12,13] retained for the present work, a third-order wave equation namely Lilley's equation,[14] the linearized Euler's equations or SNGR model.[15] All of these methods requires knowledge of the aerodynamic fluctuations.

The Lighthill analogy, which is based on the resolution of Lighthill's equation derived from the compressible Navier–Stokes equations, was the first attempt to estimate the sound radiated from a finite region of turbulent flow. This method is a very powerful and general approach to compute the acoustic radiated field although it has the limitation of assuming that the refraction effect cannot be taken into account. Using this analogy, the acoustic pressure generated by a turbulent flow is expressed as a function of the Lighthill tensor $T_{ij} \approx \rho u_i u_j$. In LES calculations only the filtered variables $\tilde{u}_i$ are known and the exact Lighthill tensor cannot be computed. Lighthill's tensor $T_{ij}^{\mathrm{LES}} = \overline{\tilde{\rho}\tilde{u}_i\tilde{u}_j}$ calculated with the basic filtered variables is often used[10,11] and interactions between resolved scales and subgrid scales are not taken into account. Piomelli *et al.*[16] proposed a correction based on LES properties to recover interactions described below and corrected Lighthill's tensor T_{ij}^{LES} by adding the subgrid scale tensor. Considering only the acoustic source term, the effects of the filtering operation have been investigated and parametrizations have been proposed. Witkowska *et al.*[10] proposed an alternative solution by identifying the acoustic intensity, respectively, generated by large scales, small scales and the term resulting from the interactions between both scales. The study of filtering and the parametrization of subgrid scale tensor has been addressed by Seror *et al.*[17] to compute the radiated acoustic pressure using Lighthill's equation for the case of decaying isotropic turbulence. These results show that this parametrization leads to reliable results when scale similarity type models are used in the representation of the acoustic field generated by the interaction between resolved- and subgrid-scales. A recent analytical development based on high Reynolds number turbulent flow performed by Rubinstein and Zhou[18] has shown the importance of the unresolved-scales in the noise production process. The present work addresses the evaluation and modeling of the

a)Author to whom correspondence should be addressed. Telephone: (+33) 01 46 73 42 71. Fax: (+33) 01 46 73 41 66. Electronic mail: sagaut@onera.fr

unresolved- and subgrid-scales contribution to the radiated noise itself when Lighthill's analogy and LES are used together for larger Reynolds number turbulent flows on the ground of *a priori* and *a posteriori* tests. The case of the sound radiated by a volume of isotropic turbulence is retained as a test case for the present study. This is an academic case, which is one of the very few examples of turbulent flow whose equivalent acoustic source has well defined properties. It appears consequently as a first step toward the derivation of fully general model. This problem has been addressed by many authors, both from a theoretical[14,19] and a numerical[10,20] point of view. Nevertheless, even for this very simple turbulent flow, the authors are not aware of any published *a posteriori* tests for subgrid models for the noise source, the previous studies being devoted to *a priori* analysis. Considering that the modeling process for the subgrid noise source should start with simple flows, which are well controlled from a theoretical and numerical point of view, isotropic turbulence appears as an mandatory first step. But, as for the modeling of usual subgrid terms, recall that the extension to more complex flows could be required to complicate the models. This point will be addressed in future works.

The mathematical formulation concerning Lighthill's equation is first presented in Sec. II. Section III is devoted to the description of the numerical method and the implementation of acoustic calculations for the study. Numerical results obtained from *a priori* tests (i.e., filtered DNS) and concerning both evaluation and modeling of the subgrid scale effects are detailed in Sec. IV. In order to assess conclusions given by the filtered DNS, *a posteriori* tests described in Sec. V have been carried out. Conclusions are presented in Sec. VI.

II. MATHEMATICAL FORMULATION

A. Governing equations

Lighthill's analogy[12,13] is a method to compute the radiated acoustic field from a finite region of turbulent flow. This analogy is based on a combination of compressible Navier–Stokes equations which leads to an inhomogeneous wave equation for the density

$$\frac{\partial^2}{\partial t^2}\rho - c_0^2\frac{\partial^2}{\partial y_i y_i}\rho = \frac{\partial^2}{\partial y_i \partial y_j}T_{ij}, \tag{1}$$

where c_0 is the constant speed of sound in the ambient medium, which is supposed to be at rest, and the Lighthill tensor T_{ij} is defined as follows:

$$T_{ij} = \rho u_i u_j + (p - c_0^2\rho)\,\delta_{ij} - \sigma_{ij}. \tag{2}$$

For high Reynolds numbers the viscous stress tensor σ_{ij} in Lighthill's tensor expression can be neglected. The quantity $(p - c_0^2\rho)$ is responsible for thermoacoustics effects[21] and will be neglected for the class flow that have been considered in this paper. Under these assumptions, the Lighthill tensor simplifies to

$$T_{ij} = \rho u_i u_j. \tag{3}$$

The solution of the Lighthill equation leads to a representation of the radiated acoustic field. Once the acoustic source term, which is zero outside the flow region, has been computed by solving the Navier–Stokes equations to compute variables ρ and u_i, the sound field generated by the turbulent motion is uniquely defined. This equation has an exact solution only for an homogeneous medium at rest, which can be obtained using the Green function. For high Reynolds number flow, a complete knowledge of the source term requires a high resolution of the flow field and then an important computational cost. A direct numerical simulation (DNS) may only be applied on simple configurations[22] and is far from addressing range of Reynolds number that have to be dealt with in practice.

B. Extension to LES

When a large-eddy simulation is performed to obtain aerodynamic fluctuations, Lighthill's equation should be derived from the filtered Navier–Stokes equations. This formalism has been presented by Seror *et al.*[17] for the compressible subsonic case. Since we are dealing with very low Mach number turbulent flows, the present simulations have been performed using the incompressible Navier–Stokes equations. As expressed in Crow's paper[23] the inconsistent incompressible approximation to Lighthill's source term is justifiable for low Mach number turbulent flow. More recently, Ristorcelli[24] has shown that the associated error term scales as the square of the Mach number. This approximation is then appropriate to compute flows which are under consideration in the present work.

In large-eddy simulation of turbulent flows, any quantity F in the flow domain V can be split into a resolved or filtered part $\overline{F}$ and an unresolved or subgrid part f through the application of a low-pass convolution filter:

$$F = \overline{F} + f, \tag{4}$$

with

$$\overline{F}(\mathbf{y}) = \int_V G_\Delta(\mathbf{y} - \xi)F(\xi)\,d\xi, \tag{5}$$

where G_Δ is the spatial kernel filter and $\Delta = \pi/k_c$ the characteristic cutoff length scale. The cutoff wave number k_c defines the limit between the low-frequency components resolved in the simulation and the remaining high-frequency components which are modeled. The kernel G_Δ is currently represented by a sharp cutoff filter, a Gaussian filter or top-hat filter for analytical development. This function is assumed to fulfill the three following constraints: constant preservation, linearity and commutativity with derivatives. A filtered Lighthill equation can then be obtained in the following two ways: by operating the combination between the filtered continuity equation and filtered momentum equation used in LES or by filtering the Lighthill equation (1). Both methods lead to the equation

$$\frac{\partial^2}{\partial t^2}\overline{\rho} - c_0^2\frac{\partial^2}{\partial y_i y_i}\overline{\rho} = \frac{\partial^2}{\partial y_i \partial y_j}\overline{T}_{ij}. \tag{6}$$

Under the assumptions of isentropic acoustic pressure fluctuations due to low Mach number and high Reynolds number turbulent flow, the filtered Lighthill tensor T_{ij} which represents the production of resolved acoustic fluctuations is then given by

$$\overline{T}_{ij}=\overline{\rho u_i u_j}=\rho_0\overline{u_i u_j}, \tag{7}$$

where ρ_0 is the flow density. As only the filtered velocity components $\overline{u_i}$ are available in LES calculations, the filtered Lighthill tensor cannot be computed and must be written as a function of filtered variables. Introducing the subgrid scale tensor τ_{ij} resulting from the nonlinearity of the convective terms and defined as

$$\tau_{ij}=(\overline{u_i u_j}-\overline{u_i}\,\overline{u_j}), \tag{8}$$

$\overline{T}_{ij}$ can be approximated by $T_{ij}^{\mathrm{LES}}=\rho_0\overline{u_i}\,\overline{u_j}$ with an inherent error T_{ij}^{SGS} which is actually the subgrid scale tensor τ_{ij} defined in Eq. (8):

$$\overline{T_{ij}}=T_{ij}^{\mathrm{LES}}+T_{ij}^{\mathrm{SGS}}=\rho_0(\overline{u_i}\,\overline{u_j}+\tau_{ij}). \tag{9}$$

The final decomposition for the full Lighthill tensor is then written as

$$T_{ij}=T_{ij}^{\mathrm{LES}}+T_{ij}^{\mathrm{SGS}}+T_{ij}'', \tag{10}$$

where T_{ij}'' is the high-frequency part of the Lighthill tensor and is not resolved in LES calculations.

The subgrid scale tensor appears naturally as a source term in the expression of the acoustic fluctuating pressure. In order to get reliable far-field noise prediction using LES calculations, this tensor must be evaluated to assess the accuracy of a prediction of the far-field noise from LES simulations.

III. NUMERICAL ALGORITHM

A. Numerical method and forcing scheme

1. Direct numerical simulation

A direct numerical simulation has been performed on a three dimensional incompressible turbulence. The dynamical equation of the Fourier-transformed velocity $\hat{u}_i(\mathbf{k},t)$ for wave vector $\mathbf{k}$ and time t, are written, following Orszag:[25,26]

$$\left(\frac{\partial}{\partial t}+\nu k^2\right)\hat{u}_i(\mathbf{k},t)=-\frac{i}{2}P_{ilm}(\mathbf{k})\int \hat{u}_l(\mathbf{p})\hat{u}_m(\mathbf{k}-\mathbf{p})d\mathbf{p}, \tag{11}$$

where

$$P_{ilm}(\mathbf{k})=k_m(\delta_{il}-k_i k_l/k^2)+k_l(\delta_{im}-k_i k_m/k^2). \tag{12}$$

Equation (11) is solved using Rogallo's[27] pseudospectral algorithm, which evaluates the convolution integral by taking the product in physical space. This algorithm does introduce aliasing errors which can be reduced by filtering the velocity field with an appropriate sharp cutoff filter. In the simulation the Fourier-transformed convective term components have been truncated for the wave number outside a sphere of radius $\frac{2}{3}N$, where N is the number of grid nodes used in each direction. The time integration has been performed using a third-order Runge–Kutta scheme. Periodic boundary conditions are applied to the solution domain which is a cubic box of length 2π, with $N^3=192^3$ equispaced grid nodes.

2. The forcing scheme

Since we are interested in a spectral analysis of the acoustic field, a statistically stationary turbulence is required.[10] In decaying isotropic turbulence, kinetic energy is dissipated after a few eddy turns over time following the $t^{-1.2}$ decay law,[28] leading then to a vanishing acoustic pressure. A spectral deterministic forcing scheme has been implemented to obtain statistically stationary velocity field. One way to generate statistically stationary turbulence is to ''force'' the large scale velocity components by artificially adding energy. This energy cascades toward the small scales and is dissipated by viscous mechanisms. Many forcing schemes have been proposed: Siggia and Patterson[29] ''froze'' the velocity Fourier amplitudes in a low-wave number band, and similarly She *et al.*[30] introduced a scheme to maintain the energy in each of the first two wave number shells constant in time. Another class of forcing scheme consists of adding an acceleration term into the momentum equation.[31] The forcing scheme used in the present work has been used by Witkowska *et al.*[10] for a similar study of sound radiated by isotropic turbulence. This forcing scheme maintains the total kinetic energy at a constant level by injecting the energy lost during the dissipation process namely ΔE in the normalized wave number band $[k_{\min},k_{\max}]=[1,5]$. The resulting forcing scheme reads

$$\hat{u}^{n+1}(k)=\beta\hat{u}^*(k), \tag{13}$$

where $\hat{u}^{n+1}(k)$ is the Fourier coefficient at time $(n+1)\Delta t$ and $\hat{u}^*(k)$ the Fourier coefficient computed by integrating the Navier–Stokes equation with $\hat{u}^n(k)$ as an initial condition, with

$$\beta=\begin{cases}\sqrt{1+\Delta E\Big/\int_{k_{\min}}^{k_{\max}}E(k)dk} & k\in[k_{\min},k_{\max}]\\ 1 \quad \text{otherwise}\end{cases}, \tag{14}$$

where ΔE is the kinetic energy loss due to dissipation during the time Δt. According to Witkowska *et al.*[10] this method ensures the continuity of the second-order derivatives in time, preventing spurious noise generation. This condition is indeed required for the present simulations: as will be shown in the following sections the acoustic source term can be expressed as a function of the second-order time-derivative of the Lighthill tensor, and the continuity of this derivative is then required.

Furthermore as the large-eddy simulation is based on parametrization of the small scales it is necessary that the small scales do not depend on the forcing scheme. The present forcing scheme appears as a post-processing of the velocity field computed after each time step, and does not appear explicitly neither in the momentum equation nor in the Lighthill equation. Its exact impact on noise production cannot be *a priori* analyzed, and will be discussed *a posteriori* when presenting DNS results (see Sec. IV A).

B. Implementation of *a priori* and *a posteriori* tests for LES

To compute the contributions of the tensors appearing in the decomposition of the Lighthill tensor, *a priori* tests have been carried out by filtering the flow field computed with a direct numerical simulation. A Gaussian filter function has been used for the present simulation, whose associated kernel in physical space G_Δ and transfer function $\hat{G}$ are, respectively,

$$G_\Delta(\mathbf{y}-\xi)=\left(\frac{6}{\pi\Delta^2}\right)^{1/2}\exp\left(\frac{-6|\mathbf{y}-\xi|}{\Delta^2}\right)^2\hat{G}(k)$$
$$=\exp\left(\frac{-\Delta^2k^2}{24}\right). \tag{15}$$

This Gaussian filter induces a smooth separation between resolved and subgrid quantities, resulting in a nonzero contribution of low frequencies to the latters. The effects of the filter have been investigated for three values of the normalized wave number k_c ($k_c=\{7,15,31\}$) leading to a representation of the field on 16^3, 32^3 and 64^3 grids, respectively. A large-eddy simulation using a parametrization of the subgrid scale tensor occurring in the Navier–Stokes equation is performed to complete the study with *a posteriori* tests. Aerodynamic fluctuations generated by stationary turbulence may be computed by resolving incompressible Navier–Stokes equations which are written as

$$\frac{\partial}{\partial t}\overline{u_i}+\frac{\partial}{\partial y_j}(\overline{u_i}\,\overline{u_j})$$
$$=-\frac{\partial}{\partial y_i}\overline{p}+\nu\frac{\partial}{\partial y_j}\left(\frac{\partial}{\partial y_i}\overline{u_j}+\frac{\partial}{\partial y_j}\overline{u_i}\right)-\frac{\partial}{\partial y_j}\tau_{ij}, \tag{16}$$

$$\frac{\partial}{\partial y_i}\overline{u_i}=0, \tag{17}$$

where τ_{ij} is the subgrid scale tensor. Then the radiated noise is deduced using the filtered Lighthill equation (6) where the associated Lighthill tensor is given by $T_{ij}=\rho_0(\overline{u_i}\,\overline{u_j}+\tau_{ij})$.

The subgrid scale tensor parametrization is required in momentum and Lighthill's equation but this parametrization is not required to be the same for both equations. It is worth noting that the subgrid terms appearing in these two equations correspond to very different physical mechanism (classical inter-scale interactions in the momentum equation and noise production for the Lighthill source term) which are associated to different mathematical formulations: simple divergence of the subgrid tensor in the momentum equations, and a second-order derivative of the same tensor in the Lighthill equation. It appears then that different models can be derived for these two terms. A ''perfect'' model for the subgrid fluctuations or the subgrid tensor τ_{ij} could theoretically be used to parametrize both effects, but previous works by Seror *et al.*[17] have shown that such a model remains to be derived. Two different models will be used in the present study. The spectral models used in momentum equations developed by Métais and Lesieur[32] leads to the subgrid scale tensor

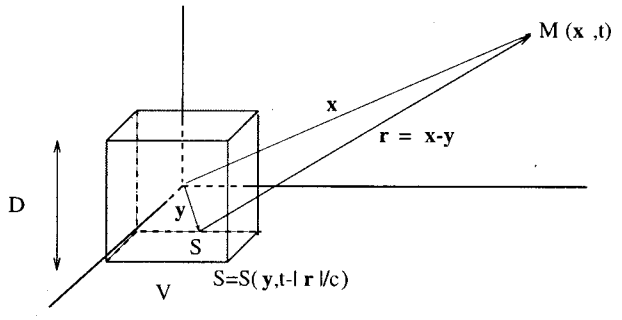

FIG. 1. Geometry of sound source radiation. V=Volume of turbulent fluid, M=observer position, $D=2\pi$.

$$\tau_{ij}=-\nu_t\left(\frac{\partial}{\partial y_i}\overline{u_j}+\frac{\partial}{\partial y_j}\overline{u_i}\right), \tag{18}$$

where $\nu_t(k)=\nu^+(k)\nu^\infty$ is the turbulent viscosity. The effective viscosity is written as follows:

$$\nu^+(k)=1+\frac{K_0^{3/2}}{\nu^\infty}15.2\,\exp(-3.03k_c/k). \tag{19}$$

Métais and Lesieur[32] developed a spectral dynamic model to compute the eddy viscosity based on an adaptation of the spectral-cusp model to kinetic-energy spectra proportional to k^{-m}. The eddy viscosity is then such as

$$\nu^\infty=0.31\frac{5-m}{m+1}K_0^{-3/2}\sqrt{\frac{E(k_c)}{k_c}}\quad\text{if } m\leqslant 3. \tag{20}$$

For $m>3$ the eddy viscosity is set equal to zero.

C. Implementation of Lighthill's analogy

The acoustic field is evaluated from Lighthill's analogy. The source term is assumed to be nonzero only in a finite region V. Then for any observer defined by the vector $\mathbf{x}$, and located outside this volume V as shown in Fig. 1, application of the Green's function formalism yields

$$\rho(\mathbf{x},t)-\langle\rho\rangle=\frac{1}{4\pi c_0^2}\int_V\frac{1}{|\mathbf{x}-\mathbf{y}|}\frac{\partial^2}{\partial y_i\partial y_j}T_{ij}\left(\mathbf{y},t-\frac{|\mathbf{x}-\mathbf{y}|}{c_0}\right)d^3y, \tag{21}$$

where $\langle\rho\rangle$ is the averaged density outside the flow domain V. This ensemble average $\langle\ \rangle$ is performed over 24 different observers located at the same distance from the center of the computational domain. As detailed by Witkowska[10] and Bastin *et al.*[7] three formulations of the solution can be expressed from Eq. (21). The formulation retained for the present work is the one successfully used by Witkowska[10] and Sarkar and Hussiani[20] in isotropic turbulence formulation and which is derived from Eq. (21) by applying the divergence theorem twice:[33]

$$\rho(\mathbf{x},t)-\langle\rho\rangle=\frac{1}{4\pi c_0^4}\frac{x_ix_j}{x^3}\int_V\frac{\partial^2}{\partial t^2}T_{ij}\left(\mathbf{y},t-\frac{|\mathbf{x}-\mathbf{y}|}{c_0}\right)d^3y. \tag{22}$$

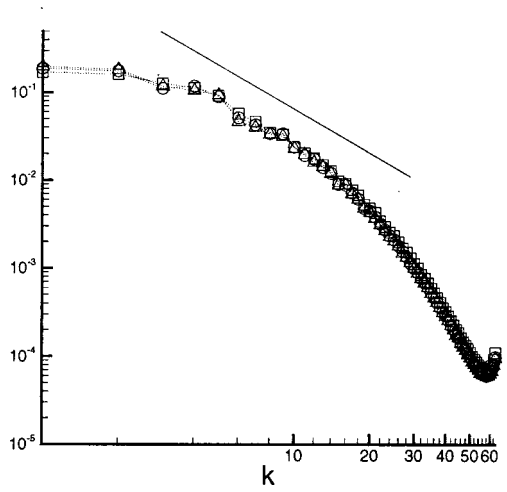

FIG. 2. Normalized energy spectrum defined as: $E^*=E(k)/\int_0^\infty E(k)]dk$ presented for three different times: □ $t^*=10.6$, △ $t^*=20.5$, ○ $t^*=35.4$, the full line represents $k^{-5/3}$.

Following the previous results presented in Refs. 10 and 20, boundary contributions appearing in Eq. (22) are suppressed in order to suppress spurious contributions due to the truncation of the source volume. This technique was shown in these references to yield very satisfactory results when computing the noise radiated by a volume of isotropic turbulence.

IV. NUMERICAL RESULTS

A. Direct numerical simulation

The velocity components have been initialized with Gaussian random numbers with the following initial energy spectrum:

$$E(k)=k^4\exp(-2k^2/k_0^2) \quad \text{where} \quad k_0=4. \tag{23}$$

The forcing scheme has been implemented after allowing the turbulence to decay until an arbitrary time ensuring that a self-similar solution is reached. The steady state is obtained at the dimensionless time $t^*=t/\tau=10.63$, where $\tau=L/u_{\rm rms}=4.05$ denotes the eddy turn over time. Acoustic computations have been carried out over approximately 25 eddy turn over time. The normalized energy spectrum is presented in Fig. 2 for three different times, which represent the initial time for acoustic computations, an intermediary time and the final time of the simulation, ensuring that the stationary state is obtained. The factor $k_{\max}\eta=1.26$, where $\eta=(\nu^3/\epsilon)^{1/4}$ is the Kolmogorov length scale, ensures that the small scales are well resolved[34] and a $k^{-5/3}$ slope is recovered on the interval $4\leqslant k\leqslant 18$. The time averaged skewness factor of the velocity derivative equals -0.47 oscillating between values -0.46 and -0.5. Since the experimental value is given to be -0.4, while simulations give $S_k\approx -0.5$, the result leads to a satisfactory agreement. Time averaged statistical turbulent quantities have been computed in terms of the three dimensional energy spectrum $E(k)$. The instantaneous energy dissipation rate, ϵ, is computed as follows:

TABLE I. Parameters and characteristic values of the flow for each simulation.

Simulation	N	Re_λ	$u_{\rm rms}$	L	λ	η
DNS	192	82.31	0.25	0.98	0.28	0.02
case 1	48	⋯	0.235	1.06	⋯	⋯
case 2	96	⋯	0.242	0.99	⋯	⋯
case 3	48	⋯	0.34	1.11	⋯	⋯
case 4	96	⋯	0.23	1.06	⋯	⋯
case 5	192	⋯	0.23	1.05	⋯	⋯

$$\epsilon=2\nu\int_0^\infty k^2E(k)dk \tag{24}$$

and the squared rms velocity is written as

$$u_{\rm rms}^2=\frac{2}{3}\int_0^\infty E(k)dk. \tag{25}$$

Other length scales used in this paper are the integral length scale L and the Taylor microscale defined λ as

$$L=\frac{\pi}{2u_{\rm rms}^2}\int_0^\infty\frac{1}{k}E(k)dk \quad \text{and} \quad \lambda^2=15\frac{\nu u_{\rm rms}^2}{\epsilon}. \tag{26}$$

The Taylor microscale Reynolds number $\mathrm{Re}_\lambda=u_{\rm rms}\lambda/\nu$ remains close to 82 during all the simulation. All averaged characteristic values and length scales are presented in Table I.

Lilley[14] emphasized some requirements for studying noise produced by isotropic turbulence at low Mach numbers on the grounds of previous works by Proudman. The first requirement is that no anisotropic effects are present in the flow. Considering the case of a volume of isotropic turbulence of size D immersed in a laminar infinite space, he recommended $L/D\ll 1$. It is observed (see Table I) that the integral length scale L is very close to 1 in all the presented simulations, with $D=2\pi$. This corresponds to the usual value of the ratio L/D (where D is the size of the computational domain) (see Eswaran and Pope[34] and Overholt and Pope[31] for a large number of examples), ensuring that the two-point correlations decay fast enough to prevent spurious coupling of the fluctuations. Because of the triperiodic nature of the simulation, there is no boundary effect between turbulence and a laminar zone, rendering the constraint less stringent than in the case considered by Lilley. The second requirement is that the turbulence must not decay significantly in the time the sound takes to cross the turbulent region, yielding $M\ll L/D$. In our case, since the turbulence is forced and does not decay, that constraint is automatically satisfied. The radiated fluctuating acoustic pressure $p'(\mathbf{x},t)=c_0^2(\rho(\mathbf{x},t)-\langle\rho\rangle)$ is then computed using DNS data by solving Eq. (22). The normalized fluctuating acoustic pressure $p^{*\prime}=p'/(u_{\rm rms}^2M_0^2)$, where $M_0=u_{\rm rms}/c_0=0.074$ is the averaged Mach number associated to the propagation outside the domain is presented in Fig. 3 as a function of the normalized time $t^*=t/\tau$ at an observer location. The signal corresponds to a general steady process rendering possible a spectral analysis of the acoustic pressure.

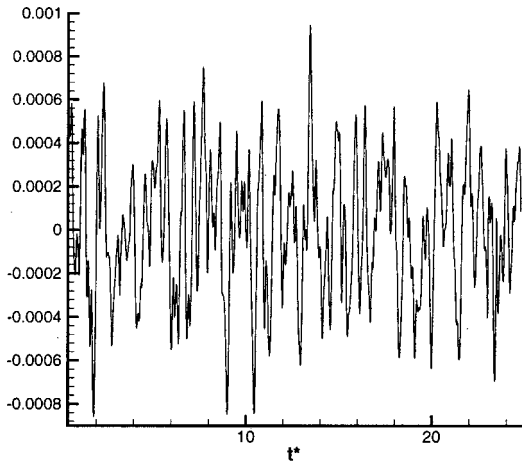

FIG. 3. Normalized fluctuating acoustic pressure defined as $p^{*\prime}=p'/(\langle\rho\rangle u_{\mathrm{rms}}^2 M_0^2)$ computed with DNS data.

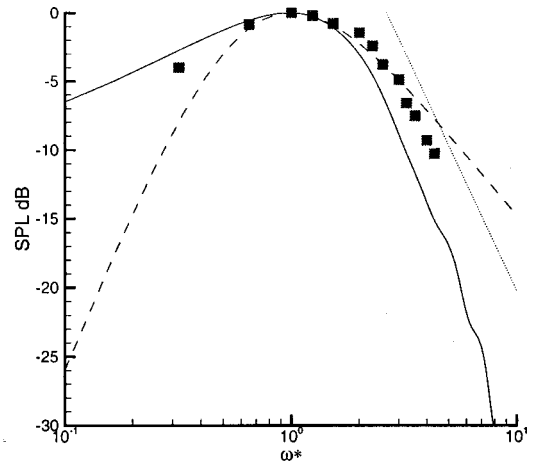

FIG. 4. Acoustic spectra computed from DNS data (——); Sarkar and Hussaini data ■; Lilley's model $\omega^{*4}(1+2\omega^{*2})^{-3}$ (— — —); Proudman's model $\omega^{*-7/2}$ (· · · ·).

The first analysis of the acoustic spectrum was given by Proudman.[19] His calculations were based on the cancellation of time correlations leading to an $\omega^{-7/2}$ slope behavior for the acoustic spectrum. More recently Lilley[14] revisited Proudman's calculation and assumed that the time correlation function depends only on the product $\Omega|\mathbf{x}-\mathbf{y}|/c_0$, where Ω is an appropriate characteristic frequency corresponding to the peak of the acoustic spectrum. Using the DNS database of Debussche *et al.*,[35] Lilley's calculation leads to the simple analytical expression for acoustic spectrum:

$$P(\omega)\propto\omega^4/(1+\omega^2/4\Omega^2)^3 \tag{27}$$

corresponding to the temporal covariance $(1+2\Omega\tau+4/3\Omega^2\tau^2)\exp(-2\Omega\tau)$. This expression satisfies the low frequency condition (the acoustic spectrum increases as ω^4) due to the temporal covariance on $\partial^4/\partial\tau^4$ developed in Lilley's model and also fits the measured results up to the high frequency ''dissipation cutoff'' (the acoustic spectrum falls as ω^{-2}). A comparison between these two models was performed by Zhou *et al.*[36] leading to Proudman's model when the Eulerian time correlations are dominated by local straining, while Lilley's result is recovered when sweeping effects by the largest energetic scales are dominant. The normalized acoustic spectrum is presented in Fig. 4 as a function of the normalized frequency $\omega^*=\omega/\omega_m$, where ω_m is the frequency at which the peak of the spectrum occurs. This peak occurs at a Strouhal number $\mathrm{St}=\omega L/u_{\mathrm{rms}}=2.15$. In their simulation Sarkar and Hussaini found a Strouhal number equal to $\mathrm{St}=3.5$ computed for a Taylor microscale Reynolds number equal to 65, while Witkowska *et al.*'s simulation leads to $\mathrm{St}=4.0$ with forced turbulence at $\mathrm{Re}_\lambda=20$. According to Lilley's theory $\mathrm{St}=2.83$ is expected while at high Reynolds numbers all simplified models of turbulence suggest that the eddies of scale close to energy containing range are responsible for the bulk of the sound generation.[37] The result found for the present simulation is then in agreement with theoretical models and leads to a smaller Strouhal number value than these obtained, respectively, by Sarkar and Hussaini and Witkowska *et al.* because of the higher Taylor microscale Reynolds number of the simulation. Nevertheless all results confirm that the noise generated by turbulence is associated to eddies smaller than energy-containing eddies and are consistent with Lighthill's and Proudman's results.

The sound pressure level is defined as $\mathrm{SPL}=20*\log(p/p_{\mathrm{ref}})$ where p_{ref} denotes the pressure associated to the peak of the signal is compared to those obtained from the Sarkar and Hussaini[20] simulation and to the analytical solution given by Eq. (27) in Fig. 4. At very low frequencies $(\omega/\omega_m\leqslant 0.6)$ discrepancies between the acoustic spectrum and Sarkar's one occur following a growth law of order $(\omega/\omega_m)^{1/2}$ while that of Sarkar and Hussaini follows a growth law of order $(\omega/\omega_m)^2$. Since the turbulence is forced at large scales the $(\omega/\omega_m)^4$ slope behavior expected by theoretical developments is not recovered. The results of Sarkar *et al.* are recovered for a normalized frequency: $0.6\leqslant\omega/\omega_m\leqslant 1.7$ with a spectral decay close to $(\omega/\omega_m)^{-2}$ for normalized frequency greater than 1. For $\omega/\omega_m\geqslant 1.7$ acoustic spectrum computed from the present simulation deviates from Sarkar and Hussaini's results by decaying more rapidly and falling down in the dissipation range with a decay law scaling as $(\omega/\omega_m)^{-7/2}$. The acoustic spectrum computed by Sarkar and Hussaini follows Lilley's model on a wider frequency range than the spectrum obtained from the present simulation before following the $(\omega/\omega_m)^{-7/2}$ law. Their results were computed from a decaying isotropic turbulence where the Strouhal number was calculated as $\mathrm{St}=\omega L_0/u_0^{\mathrm{rms}}$, the subscript 0 indicating that quantities are calculated a time $t=0$. During the simulation, the quantity u^{rms}/L is decaying in time. This indicates that the characteristic frequency is overestimated for this simulation, leading to a larger broadband acoustic spectrum than that obtained for forced turbulence where the characteristic frequency is obtained by statistical average.

Nevertheless both spectra observe the same spectral decay, ensuring that the DNS leads then to an acoustic field representation which is consistent with acoustic models and also with other simulations. This good agreement allows us to conclude on the influence of the forcing scheme on the

TABLE II. Ratio between acoustic intensities.

$\overline{I}/I$	$I^{\mathrm{LES}}/\overline{I}$	$I^{\mathrm{LES}}/\overline{I}$ Bardina's model	$I^{\mathrm{LES}}/\overline{I}$ Liu's model
16^3 32^3 64^3	16^3 32^3 64^3	16^3 32^3 64^3	16^3 32^3 64^3
0.93 0.97 0.99	0.45 0.75 0.91	0.66 0.90 0.98	0.68 0.96 1.01

noise generation. It strongly modifies the acoustic properties of the lowest resolved frequencies, yielding a 1/2 slope, but the modes located after the kinetic energy spectrum peak are not polluted, leading to the observed good agreement. Since the maximum of noise production is due to modes located after that peak and since we are interested in LES with a cutoff located in the inertial range, the present forcing scheme can be retained. The same conclusion was given by Witkowska.

B. *A priori* evaluation of subgrid scale tensor contribution to Lighthill's tensor

To analyze high frequency and subgrid contributions of the acoustic source term to the radiated noise, a comparison between acoustic quantities computed from all parts occurring in the decomposition Eq. (10) has been carried out.

In Table II, ratios between the acoustic intensity I computed from the full Lighthill tensor T_{ij} and acoustic intensity I computed from the filtered Lighthill tensor $\overline{T}_{ij}$ have been evaluated for all grids. These ratios show that the contribution to the full radiated noise generated by the high frequency part of acoustic tensor T''_{ij} remains less than 10% in all cases. In Table III ratios between turbulent scales and the mesh size are presented showing that for all values of k_c used the integral scale is well resolved, i.e., $\Delta \leqslant L$. As the noise is generated by scales smaller than the integral scale this condition must be restricted to $\Delta \leqslant L/\mathrm{St}$, where $1/\mathrm{St} = 0.47$ in the present simulation, and according to all values reported in Table III this condition is satisfied on all grids. This ensures that the scales responsible for the noise are well resolved. Comparison between spectra computed from the full Lighthill tensor and the filtered one in Fig. 5 shows that the acoustic spectrum hardly changes when the high frequency part of the acoustic source term is not taken into account. This result is in agreement with those obtained by Seror *et al.*[17] ensuring that the use of large-eddy simulation is suitable when it is used together with Lighthill's analogy and when the mesh size satisfies the condition discussed above.

The spectral decay of $\omega^{-7/2}$ is recovered in the same frequency range while discrepancies between acoustic spectra occur for higher frequencies. The acoustic spectrum decays more rapidly when the Strouhal number $\mathrm{St} \geqslant 6$ as larger cutoff wave number values are considered. When the low frequency part of Lighthill's tensor is taken into account (i.e., $\overline{u_i u_j}$) the resulting energy spectrum is computed as a function of $\widehat{u_i u_i} \hat{G}_\Delta$. In Fig. 6 these spectra are presented showing that the filter does not modify significantly the inertial range where $k^{-5/3}$ slope is recovered in accordance with Lilley's model and Zhou and Rubinstein[36] calculations.

Since the high frequency part of the acoustic source term can be neglected in all cases, the importance of the noise radiated by the subgrid modes must be estimated. It has been shown by Seror *et al.*[17] that subgrid scale tensor has a significant contribution to the radiated noise. In Table II the ratio between acoustic intensity computed from the resolved Lighthill tensor (namely I^{LES}) and $\overline{I}$ has been calculated in all cases. A large contribution of intensity generated by the subgrid scales is observed. This contribution reaches 55% for 16^3 case. In order to resolve the eddies associated to the peak

TABLE III. Parameters and characteristic values of the flow.

k_c	7	15	31
$\overline{\Delta}/\eta$	22.44	10.47	5.07
$\overline{\Delta}/\lambda$	1.31	0.70	0.34
$\overline{\Delta}/L$	0.40	0.20	0.10

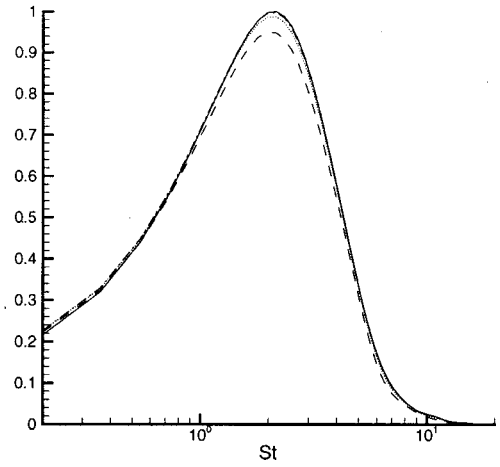

FIG. 5. Comparison between acoustic spectra computed from: DNS data (-); filtered Lighthill's tensor on 16^3 nodes (— — —); filtered Lighthill's tensor on 32^3 (· · · ·); filtered Lighthill's tensor on 64^3 (—·—·—·—).

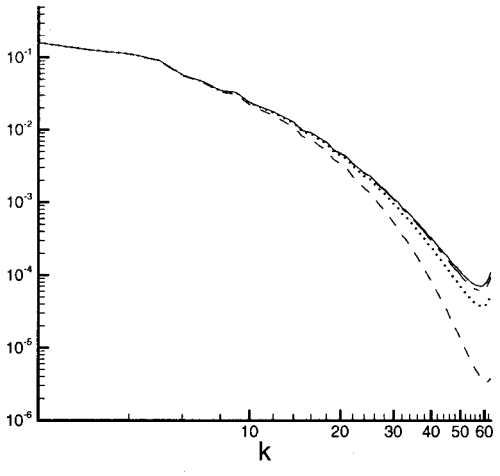

FIG. 6. Comparison between energy spectrum computed from DNS data: $E(k)$ (——) and energy spectrum associated to the filtered Lightill tensor $E(k)G_\Delta(k)$ on (— — —) 16^3 nodes; (· · · ·) 32^3 nodes; (—·—·—·—) 64^3 nodes.

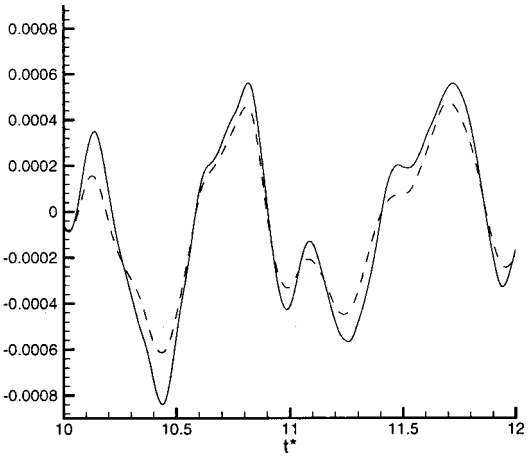

FIG. 7. Comparison between acoustic pressures respectively associated to the filtered Lighthill tensor (——) and the resolved Lighthill tensor (— — —) on 32^3 grid.

of the acoustic spectrum the condition $\Delta/L \leqslant 0.47 = 1/\mathrm{St}$ is required, for this grid $(16^3)\Delta/L = 0.4$ is obtained indicating that the smallest resolved eddies are very close to those associated to the peak of the acoustic spectrum.

When the subgrid scale effects representing the interaction between the resolved and the unresolved structures are not taken into account, the results obtained are very far from the solution computed from the low frequency part of the acoustic source term. The largest error is observed as expected for the lowest value of k_c (i.e., 16^3) used for the simulation. On the 32^3 grid mesh representation presented in Fig. 7, the subgrid contribution is still significant. Errors occur for both amplitude and phase of the acoustic signal indicating an important effect of the subgrid scale.

The comparison between acoustic spectra of the quantity $(p/p_{\mathrm{ref}})^2$ where p_{ref} is the amplitude of the peak of the spectrum for DNS case and the pressure p is computed from the full Lighthill tensor and from the resolved one is presented in Fig. 8. Important discrepancies concerning acoustic spectrum computed on 16^3 and 32^3 grids occur while the solution on

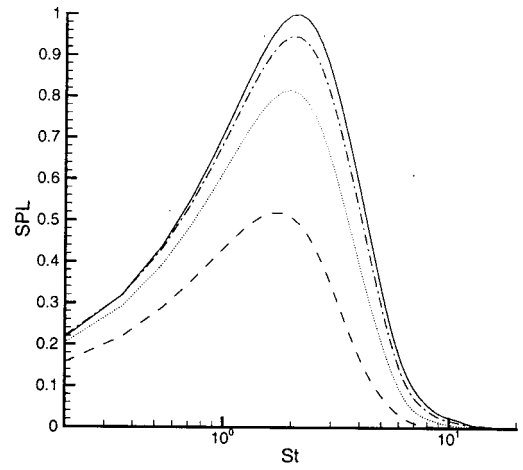

FIG. 8. Comparison between acoustic spectra computed from: the full Lighthill tensor (——); the resolved Lighthill tensor on 16^3 (— — —), on 32^3 (· · · ·), on 64^3 (—·—·—·—) grids.

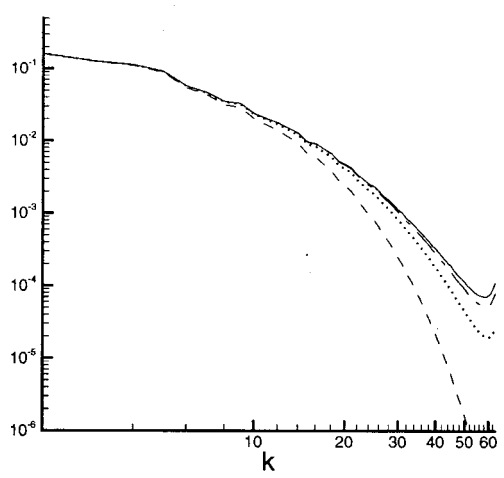

FIG. 9. Comparison between energy spectrum computed from DNS data: $E(k)$ (——) and energy spectrum associated to the filtered Lightill tensor $E(k)G_\Delta^2(k)$ on (— — —) 16^3 nodes; (· · · ·) 32^3 nodes; (—·—·—·—) 64^3 nodes.

64^3 nodes remains close to the DNS result. As the filtered Lighthill tensor allows to recover the behavior expected by Proudman's theory, the resolved Lighthill tensor does not for the two lowest values of k_c as shown in Fig. 8. In the frequency range $\mathrm{St} \in [2,6]$ where Proudman's model was recovered, the acoustic spectrum decreases more rapidly when the resolved Lighthill tensor is used for the computation. Moreover the peak of the acoustic spectrum for these two cases has been shifted to the lowest frequency leading now to $\mathrm{St} = 1.8$ for the 16^3 case and a 2.0 for the 32^3 case while $\mathrm{St} = 2.15$ was expected (Fig. 8). As suggested by the intensity ratio $I^{\mathrm{LES}}/\overline{I} = 0.91$ on the 64^3 grid the acoustic spectrum remains close to the DNS one. When a LES is performed the resulting kinetic energy spectrum is computed as a function of $u_i u_j \hat{G}_\Delta^2$. These spectra are presented in Fig. 9 showing that the inertial range is still there for cutoff wave number values considered. As the decay of Eulerian time correlations was dominated by large scale straining according to Zhou *et al.*,[36] the use of the resolved Lighthill tensor does not recover reliable results indicating that the subgrid scale tensor should be parametrized in both cases 16^3 and 32^3 mesh grid to get reliable results for the acoustic field.

C. Parametrization of the Lighthill subgrid scale tensor

In order to recover reliable results concerning both acoustic intensity and Strouhal number when LES and Lighthill's tensor are used together, a parametrization of the subgrid Lighthill tensor must be performed. Two models have been tested for the compressible case:[17] a subgrid scale model of eddy viscosity type, like the Smagorinsky model[38] and a scale similarity type model, like the Bardina model.[39,40] The Bardina model led to better results than the Smagorinsky model and for the present simulations scale similarity models have been retained. Subgrid Lighthill's tensor parametrization with Bardina's model has been chosen leading to

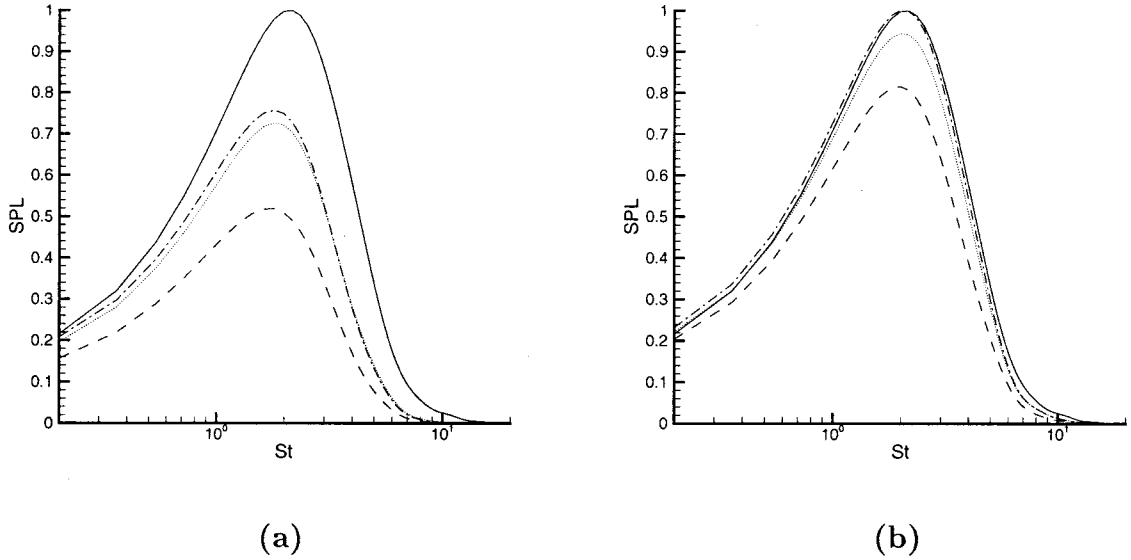

FIG. 10. Comparison between acoustic spectra computed from DNS data and filtered DNS on 16^3 nodes (a) and 32^3 nodes (b): the full Lighthill tensor (——); the resolved Lighthill tensor (— — —); the resolved Lighthill tensor with a correction given by Bardina's model (· · · ·); the resolved Lighthill tensor with a correction given by Liu's model (—·—·—·—).

$$T_{ij}^{\mathrm{SGS}} = m_{ij} = \overline{\overline{u_i u_j}} - \bar{u}_i \bar{u}_j . \tag{28}$$

The Bardina model is indeed a theoretical model, which cannot be applied if the analytical form of the filter is unknown. Liu *et al.*[41] have developed a more general scale similarity model written as follows:

$$m_{ij} = C_L(\widetilde{u_i u_j} - \tilde{u}_i \tilde{u}_j), \tag{29}$$

where $C_L = 0.45$, *bar* still denotes a filter at scale $\bar{\Delta}$ associated to the mesh size and *tilde* denotes a filter at scale $2\bar{\Delta}$.

The ratio between the acoustic intensity computed from the resolved Lighthill tensor corrected with subgrid tensor (namely $\mathbf{I}^{\mathrm{LES}}$) and the filtered acoustic intensity is presented in Table II. In all cases and for both models significant improvements are observed. Nevertheless Liu's model seems to recover better results than Bardina's one. The ratio reaches 96% and more than 99% for, respectively, 32^3 and 64^3 grid nodes confirming that scale similarity models are suitable to recover the noise generated by the subgrid scales. Acoustic spectra computed from the full Lighthill tensor, the resolved Lighthill tensor and the resolved Lighthill tensor corrected with both models are presented in Figs. 10(a) and 10(b), respectively, for the 16^3 grid and the 32^3 grid. As the solution on the 16^3 grid was far from the results given by DNS improvements concerning the Strouhal number are indeed observed leading to St=1.9 for both models while St=1.8 was found without model as shown in Fig. 10(a). This result indicates that model effects are strong even if the solution is far away from the expected one. On the 32^3 grid, both models also lead to significant improvements for the spectral density. The acoustic spectrum in Fig. 10(b) computed using the corrected Lighthill tensor remains close to DNS results after the peak of the acoustic spectrum while without subgrid correction it was falling down. As higher frequencies are considered the improvements are less significant and the acoustic spectrum moves away from the expected solution but still gives better results than without the model. Discrepancies between the Strouhal number associated to the peak of the acoustic spectrum are smaller. The measured Strouhal number is St=2.12, while St=2.0 has been found when subgrid effects were not taken into account. These values are very close to the St=2.15 obtained in the full DNS. Results obtain on the 64^3 grid dealing with the associated Strouhal number are insensitive to the correction of the Lighthill tensor. This demonstrates that the model acts weakly when the solution obtained by LES is close to these obtained by DNS. The subgrid scale model of scale similarity type offers a good issue to parametrize subgrid tensors occurring in the filtered Lighthill equation. These models make it possible to recover a part of the acoustic intensity that is not taken into account as was shown by results on the 16^3 and 32^3 grids and also do not introduce overprediction of the radiated noise when subgrid model is not really required.

V. LARGE-EDDY SIMULATION: *A POSTERIORI* TESTS

The formalism presented in Sec. II has been illustrated by an *a priori* test based on direct numerical simulation because it was the best way to analyze the contributions of all of Lighthill's tensors appearing in the decomposition given by Eq. (10). The effects of the mesh size have been parametrized by a Gaussian filter function. When a real large-eddy simulation is carried out the study differs from the filtered DNS by several points. First of all the filter kernel and the cutoff wave number value are not known exactly. Moreover aerodynamic fluctuations are computed using a parametrization of the subgrid scale tensor appearing in the filtered Navier–Stokes equation while the exact form of the subgrid tensor was used in the previous study. To compare results obtained by direct numerical simulation and those obtained

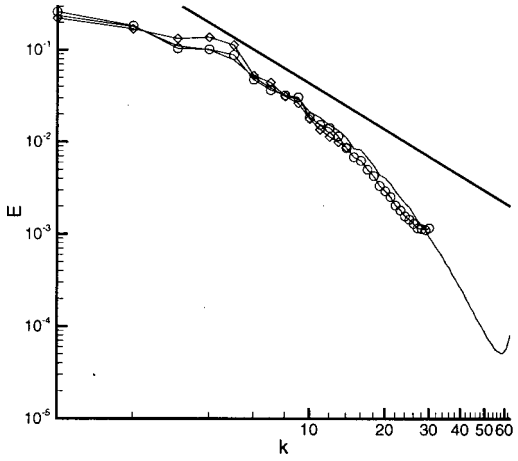

FIG. 11. Kinetic energy spectrum: full line DNS; ◇ case 1, ○ case 2.

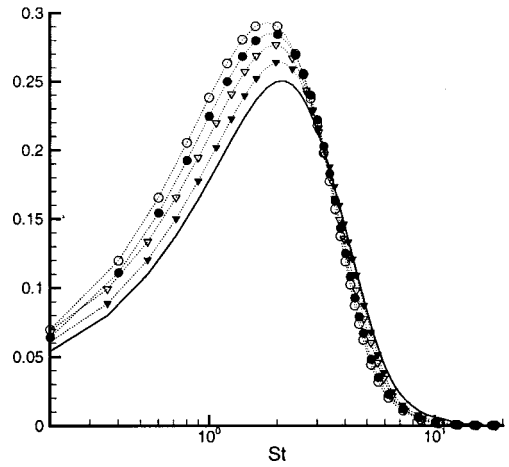

FIG. 12. Power spectral density computed from: DNS, full line; filtered DNS on 32^3 grid, without correction ▽, with correction ▼; case 1, without correction ○, with correction ●.

when real LES is performed, large-eddy simulations on 32^3 and 64^3 grids have been carried out using the same turbulent parameters as those used for the DNS (i.e., the same eddy viscosity and same kinetic energy). The forcing scheme used is the same as those implemented for the DNS and the value of kinetic energy is equal to these resulting from the filtered DNS on the corresponding grid. Simulations are, respectively, referred to as case 1 and case 2 for the Métais and Lesieur[32] model on, respectively, the 32^3 or 64^3 grids. Kinetic energy spectra for these two simulations are presented in Fig. 11 and compared to the DNS results. It is seen that simulations performed by LES led to kinetic energy spectrum which is very close to the DNS one. Parameters and statistics concerning these simulations are reported in Table I.

Discrepancies between values obtained for the Strouhal number associated to the peak of the spectrum are reported in Table IV. The results indicate that the scales responsible for the noise are not resolved in the same way whether the filtered DNS or LES is considered. When Liu's model is used to parametrize the subgrid Lighthill tensor, significant improvements are observed for all simulations by moving the peak of the spectrum to higher frequencies.

In Fig. 12 and Fig. 13 the power spectral density computed from the resolved Lighthill tensor with and without correction is plotted as a function of St and compared to those obtained by DNS and filtered DNS. Discrepancies observed between LES and filtered DNS concern both the position of the peak of the spectrum and its amplitude. Discrepancies on the amplitude of the peak indicate that the acoustic energy is not distributed on the same frequency range whether DNS is filtered or LES is performed. This result suggests that the effective filter function is not the same for all simulations and that the smallest scale resolved (i.e., these associated to the highest available frequency) differ whether the simulation is performed. When a parametrization of the Lighthill subgrid scale tensor is added to the resolved Lighthill tensor, interactions between the resolved and the unresolved scales are taken into account such that a decay of the amplitude of the peak is observed leading to results closer to those obtained by DNS, as shown in Fig. 12 and Fig. 13. Results obtained from these simulations are consistent with those obtained from the filtered DNS and these discrepancies are especially due to the filtering function, indicating that the subgrid scale tensor used in the momentum equation does not introduce spurious effect.

The main interest of LES is to compute high Reynolds number turbulent flows. To extend the range of the study to purely convective regimes, LES have been performed setting

TABLE IV. Strouhal number obtained for LES simulations without/with subgrid Lighthill's tensor.

Lighthill's tensor	T^{LES} St	$T^{\mathrm{LES}}+T^{\mathrm{SGS}}$ St
case 1	1.80	1.9
case 2	2.10	2.2
case 3	1.55	1.67
case 4	2.17	2.28
case 5	2.22	2.3

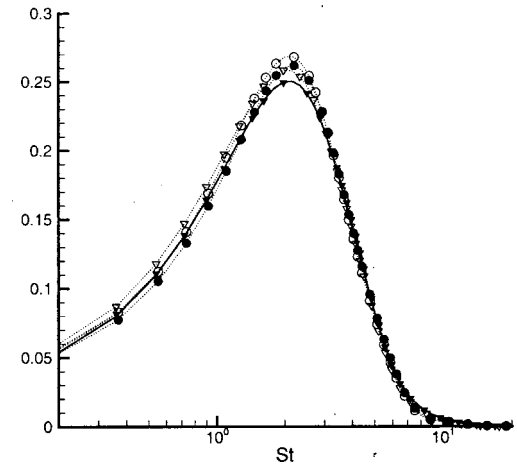

FIG. 13. Power spectral density computed from: DNS, full line; filtered DNS on 64^3 grid, without correction ▽, with correction ▼; case 1, without correction ○, with correction ●.

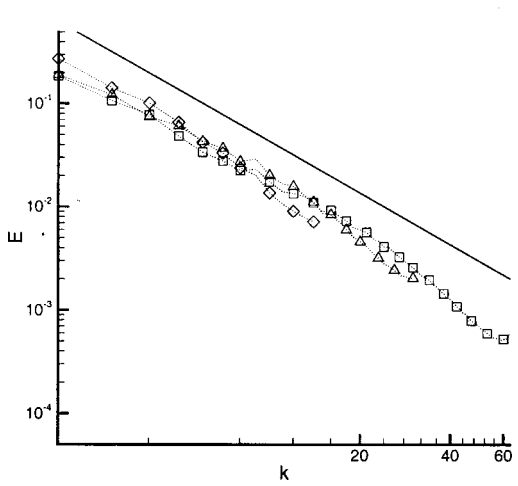

FIG. 14. Kinetic energy spectrum: case 3 ◇; case 4 △; case 5 □; the full line represents $k^{-5/3}$.

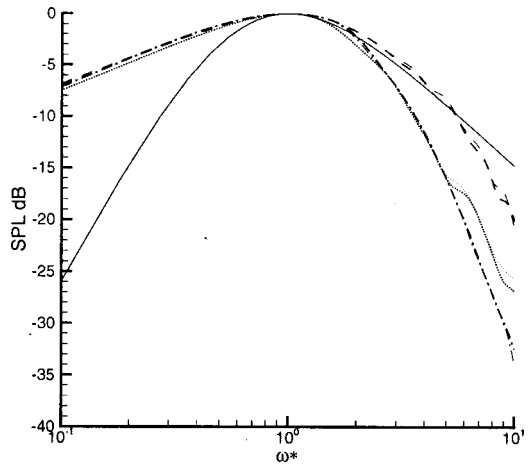

FIG. 16. Comparison between sound pressure level (dB) case 3 (—·—·—·—); case 4 (· · · ·); case 5 (— — —). The thin lines represent the power spectral density when Lighthill's tensor is corrected with Liu's model. The full line is the Lilley model.

the molecular eddy viscosity to zero such that the diffusive effect are only governed by the subgrid scale model of eddy viscosity type. These simulations have been carried out using the Métais and Lesieur[32] spectral model described in Sec. III. These simulations are referred to as case 3, case 4 and case 5 for simulations performed on, respectively, 32^3, 64^3 or 128^3 grids. Kinetic energy spectrum obtained for these simulations are presented in Fig. 14 showing that a $k^{-5/3}$ is recovered and inertial kinetic-energy range is obtained up to the cutoff wave number. Parameters and statistics concerning these simulations are reported in Table I. The Strouhal number values obtained are reported in the Table IV. All of these values remain close to those obtained with the previous study indicating that the position of the peak of the acoustic spectrum does not depend on the Reynolds number. The spectral density has been computed as a function of the Strouhal number and is presented in Fig. 15. The mesh size used and consequently the inertial range width represent important parameters for such simulations. As the mesh size is refined (case 5) the highest accessible frequency is growing up leading to an enrichment of the high frequency part of the acoustic spectrum. As observed for other simulation the use of a parametrization for the subgrid Lighthill tensor introduce significant corrections concerning both amplitude and position of the peak. As explained in Sec. IV A, the theoretical model based on the assumption of an infinite Reynolds number flow predicts a ω^{-2} spectral decay[14] or $\omega^{-4/3}$ according to Zhou and Rubinstein.[36] In Fig. 16 the SPL have been plotted as a function of the normalized frequency ω^* and the results are compared to Lilley's model. Only case 5 leads to results close to Lilley's model. The acoustic spectrum recovers an ω^{-2} over a significant frequency range for this case indicating that the width of the inertial kinetic-energy range has an important signification. The model developed by Zhou and Rubinstein[36] was indeed based on the assumption of an infinite inertial kinetic-energy range and led to $\omega^{-4/3}$ spectral decay for the acoustic spectrum.

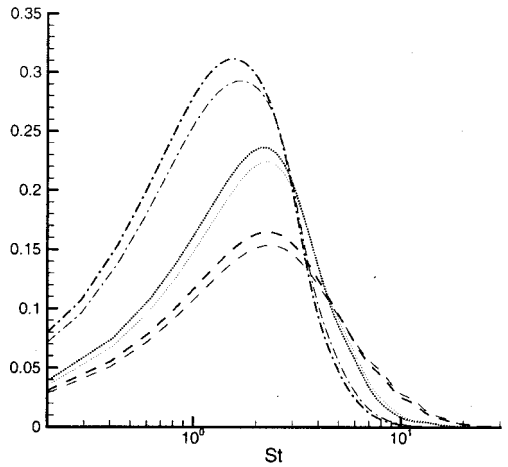

FIG. 15. Comparison between power spectral density case 3 (—·—·—·—); case 4 (· · · ·); case 5 (— — —). The thin lines represent the power spectral density when Lighthill's tensor is corrected with Liu's model.

The previous study concerning filtered DNS has shown that the acoustic intensity is also corrected when subgrid scale Lighthill's tensor is taken into account. To analyze the subgrid scale contribution to the acoustic intensity, the ratio $\mathbf{I}/I^{\mathrm{LES}}$ as computed has a function of the cutoff wave number and is presented in Fig. 17. Comparison between results obtained, respectively, by filtered DNS and LES indicates that the contribution of subgrid scales to the acoustic intensity depends on the mesh size used for the simulation.

VI. CONCLUDING REMARKS

Computation of acoustic quantities by filtering DNS data show that a parametrization of the subgrid scale tensor occurring in Lighthill's equation is required to recover reliable results for the acoustic field. The study was especially based on the radiated acoustic spectrum. The use of LES shifts the peak of the spectrum toward low frequencies and does not allow the acoustic intensity generated by the high frequency part of the acoustic source term to recover. Subgrid scale models of scale similarity type are suitable to recover the acoustic intensity lost in the filtering procedure and to im-

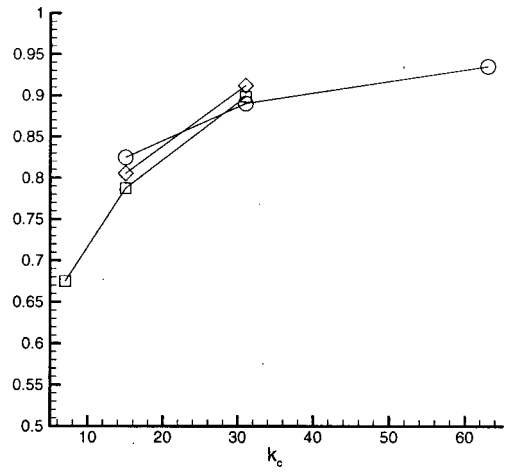

FIG. 17. Acoustic intensity ratio $\mathbf{I}/I^{\mathrm{LES}}$ computed from Liu's model for all simulations: Filtered DNS □; case 1 and case 2 ◇; case 3, case 4 and case 5 ○.

prove the prediction of the location of the peak of acoustic spectrum with respect to DNS results. LES have been performed using a spectral eddy-viscosity model. The comparison between filtered DNS and LES led to small discrepancies when dealing with acoustic spectra. This is especially due to the difference between the filter kernel used for *a priori* tests and the effective filter of the *a posteriori* tests. As all theoretical models are based on infinite Reynolds number turbulent flow, the extension to LES in the vanishing viscosity case performed on several grids shows that these models are recovered only if the inertial kinetic-energy range is large enough. In all cases the parametrization give suitable and consistent results: the model introduced a correction to the acoustic intensity which depends on the computational grid and yields a shift of the peak of acoustic toward larger frequencies for all considered cases.

[1]H. S. Ribner, ''Quadrupole correlations governing the pattern of jet noise,'' J. Fluid Mech. **38**, 1 (1969).
[2]M. E. Goldstein and B. Rosenbaum, ''Effects of anisotropic turbulence on aerodynamic noise,'' J. Acoust. Soc. Am. **54**, 630 (1973).
[3]W. Béchara, P Lafon, C. Bailly, and S. Candel, ''Application of a $k-\epsilon$ model to the prediction of noise for simple and coaxial free jets,'' J. Acoust. Soc. Am. **97**, 3518 (1995).
[4]C. K. W. Tam, ''Computational aeroacoustics: Issues and methods,'' AIAA J. **33**, 1788 (1995).
[5]S. K. Lele, ''Computationnal aeroacoustics: A review,'' in AIAA Paper 97-0018 (1997).
[6]J. Freund, T. Colonius, and K. Mohseni, ''Acoustic sources in a turbulent jet: A direct numerical simulation,'' in AIAA Paper 99-1858 (1999).
[7]F. Bastin, P. Lafon, and S. Candel, ''Computation of jet mixing noise due to coherent structures: The plane jet case,'' J. Fluid Mech. **335**, 261 (1997).
[8]C. Bailly, S. Candel, and P. Lafon, ''Prediction of supersonic jet noise from a statistical acoustic model and a compressible turbulence closure,'' J. Sound Vib. **194**, 219 (1996).
[9]C. Bailly, P. Lafon, and S. Candel, ''Subsonic and supersonic jet noise prediction from statistical source models,'' AIAA J. **35**, 1688 (1997).
[10]A. Witkowska, D. Juvé, and J. G. Brasseur, ''Numerical study of noise from isotropic turbulence,'' J. Comput. Acoust. **5**, 317 (1997).
[11]E. Manoha, B. Troff, and P. Sagaut, ''Trailing edge noise prediction using large-eddy simulation and acoustic analogy,'' AIAA J. **38**, 575 (2000).
[12]M. J. Lighthill, ''On sound generated aerodynamically. Part I: General theory,'' Proc. R. Soc. London, Ser. A **211**, 564 (1952).
[13]M. J. Lighthill, ''On sound generated aerodynamically. Part II: Turbulence as a source of sound,'' Proc. R. Soc. London, Ser. A **222**, 1 (1954).
[14]G. M. Lilley, ''The radiated noise from isotropic turbulence,'' Theor. Comput. Fluid Dyn. **6**, 281 (1994).
[15]C. Bailly and D. Juvé, ''A stochastic approach to compute subsonic noise using linearized Euler's equations,'' in AIAA Paper 99-1872 (1999).
[16]U. Piomelli, G. L. Streett, and S. Sarkar, ''On the computation of sound by large-eddy simulations,'' J. Eng. Math. **32**, 217 (1997).
[17]C. Seror, P. Sagaut, C. Bailly, and D. Juvé, ''Subgrid scale contribution to noise production in decaying isotropic turbulence,'' AIAA J. **38**, 1795 (2000).
[18]R. Rubinstein and Y. Zhou, ''Characterization of sound radiated by unresolved scales of motion in computational aeroacoustics,'' Technical Report 99/39, ICASE (1999).
[19]I. Proudman, ''The generation of sound by isotropic turbulence,'' Proc. R. Soc. London, Ser. A **214**, 119 (1952).
[20]S. Sarkar and M. Y. Hussaini, ''Computation of the sound generated by isotropic turbulence,'' Technical Report 93-74, ICASE (1993).
[21]D. G. Crighton, A. P. Dowling, J. E. Ffowcs Williams, M. Heckl, and F. G. Leppington, *Modern Methods in Analytical Acoustics* (Springer Verlag, New York, 1992).
[22]P. Moin and K. Mahesh, ''Direct Numerical Simulation: A tool in turbulence research,'' Annu. Rev. Fluid Mech. **30**, 539 (1998).
[23]S. C. Crow, ''Aerodynamic sound emission as a singular perturbation problem,'' Stud. Appl. Math. **49**, 21 (1970).
[24]J. R. Ristorcelli, ''A closure for the compressibility of the source terms in Lighthill's acoustic analogy,'' Technical Report 97-44, ICASE (1997).
[25]S. A. Orszag, ''Numerical simulation of incompressible flows within simple boundaries: I. Galerkin (spectral) representations,'' Stud. Appl. Math. **2**, 293 (1971).
[26]S. A. Orszag, ''Numerical simulation of incompressible flows within simple boundaries: II. Accuracy,'' J. Fluid Mech. **49**, 75 (1971).
[27]R. S. Rogallo and P. Moin, ''Numerical simulation of turbulent flows,'' Annu. Rev. Fluid Mech. **16**, 99 (1984).
[28]G. Comte-Bellot and S. Corrsin, ''The use of contraction to improve the isotropy of grid-generated turbulence,'' J. Fluid Mech. **25**, 657 (1966).
[29]E. D. Siggia and G. S. Patterson, ''Intermittency effects in a numerical simulation of stationarity three-dimensional turbulence,'' J. Fluid Mech. **86**, 567 (1978).
[30]Z.-S. She, E. Jackson, and S. A. Orszag, *Statistical Aspect of Vortex Dynamics in Turbulence, New Perspectives in Turbulence* (Springer, Berlin, 1991).
[31]M. R. Overholt and S. B. Pope, ''A deterministic forcing scheme for direct numerical simulations of turbulence,'' Comput. Fluids **27**, 11 (1998).
[32]O. Métais and M. Lesieur, ''Spectral large-eddy simulation of isotropic and stably stratified turbulence,'' J. Fluid Mech. **256**, 157 (1992).
[33]W. K. Blake, *Mechanics of Flow-Induced Sound and Vibration* (Academic, New York, 1986), Vol. 1.
[34]V. Eswaran and S. B. Pope, ''An examination of forcing in direct numerical simulations of turbulence,'' Comput. Fluids **16**, 257 (1988).
[35]A. Debussche, T. Dubois, and R. Temam, ''The Nonlinear Galerkin Method: A multi-scale method applied to the simulation of homogeneous turbulent flows,'' Technical Report 93/93, ICASE (1993).
[36]Y. Zhou and R. Rubinstein, ''Sweeping and straining effects in sound generation by high Reynolds number isotropic turbulence,'' Phys. Fluids **8**, 647 (1996).
[37]G. M. Lilley, ''The radiated noise from isotropic turbulence with applications to the theory of jet noise,'' J. Sound Vib. **190**, 463 (1996).
[38]J. Smagorinsky, ''General circulation experiments with primitive equations. I: The basic experiment,'' Mon. Weather Rev. **91**, 99 (1963).
[39]J. Bardina, J. H. Ferziger, and W. C. Reynolds, ''Improved subgrid scale models for Large-Eddy Simulation,'' in AIAA Paper 80-1357 (1980).
[40]J. Bardina, J. H. Ferziger, and W. C. Reynolds, ''Improved turbulence models based on Large-Eddy Simulation of homogeneous, incompressible, turbulent flows,'' Technical Report TF-19, Thermosciences Division, Dept. Mechanical Engineering, Stanford University (1983).
[41]S. Liu, C. Meneveau, and J. Katz, ''On the properties of similarity subgrid-scale models deduced from measurements in a turbulent jet,'' J. Fluid Mech. **275**, 83 (1994).